Model Order Reduction of 1D Diffusion Systems Via Residue Grouping

Kandler A. Smith
Center for Transportation Technologies and Systems,
National Renewable Energy Laboratory,
Golden, CO 80401

Christopher D. Rahn[1]
e-mail: cdrahn@psu.edu

Chao-Yang Wang

Department of Mechanical and Nuclear Engineering,
The Pennsylvania State University,
University Park, PA 16802

A model order reduction method is developed and applied to 1D diffusion systems with negative real eigenvalues. Spatially distributed residues are found either analytically (from a transcendental transfer function) or numerically (from a finite element or finite difference state space model), and residues with similar eigenvalues are grouped together to reduce the model order. Two examples are presented from a model of a lithium ion electrochemical cell. Reduced order grouped models are compared to full order models and models of the same order in which optimal eigenvalues and residues are found numerically. The grouped models give near-optimal performance with roughly $1/20$ *the computation time of the full order models and require 1000–5000 times less CPU time for numerical identification compared to the optimization procedure.*
[DOI: 10.1115/1.2807068]

Keywords: model order reduction, residue grouping, diffusion, system identification, Karhunen–Loève transform

1 Introduction

In the model-based control of complex or large scale systems, model order reduction enables efficient controller designs. Various reduction techniques decompose a mathematical model into modes and sort those modes based on dominance (either magnitude or speed), controllability, or observability [1–3]. Unimportant modes may be discarded or, in the case of fast modes, retained as static gains. Thermal fluid systems, exhibiting temporal and spatial dependencies governed by partial differential equations (PDEs), are infinite dimensional, making the identification of an accurate low order model difficult [4]. The present work focuses on parabolic PDE system models obtained from mass or energy conservation equations with diffusional transport. Examples include chemical vapor deposition systems [5], snap curing ovens [6], and electrochemical power systems [7,8].

The response of parabolic PDE systems is generally dominated by a finite number of slow modes and, for control purposes, the eigenspectrum of the spatial differential operator can be partitioned into finite-dimensional (possibly unstable) slow and infinite-dimensional stable fast subspaces [9]. Using this concept, Christophides and Daoutidis [10] developed a general approach for robust control of quasilinear parabolic PDE systems. Galerkin's method approximates the PDE system as a system of ordinary differential equations (ODEs), with the ODE system truncated via singular perturbations. Bhikkaji and Söderström also reduced the order of 1D [11] and 2D [12] diffusion systems via modal truncation.

A drawback of the Galerkin and collocation and similar methods is that admissible functions must be identified prior to application of the method, limiting them to systems defined on regular domains. It is often unclear a priori which function or method will most efficiently represent a particular problem [13]. Spatial discretization methods such as finite difference and finite element, widely applicable to both regular and irregular domains, generally result in a high order model [10,14]. The Karhunen–Loève decomposition [15], combined with the method of snapshots [16], provides an alternative numerical approach, identifying "empirical" eigenfunctions using time simulation results from a high order spatial discretization model. With the dominant eigenfunctions employed as basis functions in a Galerkin procedure, the low order model accurately represents [14] and controls [17] the system.

In the present investigation, empirical shape functions are extracted directly from a finite element or finite difference model and used to assemble a model in eigenvalue/residue series form. Model order is reduced by grouping or lumping together modes with similar eigenvalues. As with the Karhunen–Loève Galerkin procedure, eigenvalue decomposition is a necessary step in generating a reduced order model; however, in the present investigation, the finite element model itself is decomposed, rather than the field variable time response, eliminating the need for time simulation. The proposed approach, equally applicable for reduction of analytical solutions, provides intuition as to the connection between high order exact solutions and low order empirically fitted models.

2 Model Order Reduction Framework

We seek to generate a reduced order model (ROM) whose output response $y^*(x,t)$ accurately approximates the full order model (FOM) output response $y(x,t)$ for any arbitrary input $u(t)$. In the Laplace domain, we have input $U(s)$, FOM output $Y(x,s)$, and ROM output $Y^*(x,s)$. We restrict the work to systems with a steady state, that is, $\lim_{s\to 0} Y(x,s)/U(s)$ is finite. Reduction is performed in the frequency domain with design criteria of correct steady state and $\|Y^*(x,j\omega)-Y(x,j\omega)\| < \alpha \,\forall\, \omega \in [0, 2\pi f_c]$, where f_c is the desired model bandwidth.

Distributed L^2_Ω and L^∞_Ω norms,

$$L^2_\Omega = \left[\int_0^\infty \int_\Omega |\hat{y}(x,t)|^2 dx dt\right]^{1/2}$$

$$L^\infty_\Omega = \max_{\Omega, t\in[0,\infty)} |\hat{y}(x,t)| \tag{1}$$

quantify time domain error, $\hat{y}=y^*-y$, across spatial domain $\Omega=\{x: x\in[0,1]\}$.

[1]Corresponding author.

Contributed by the Dynamic Systems, Measurement, and Control Division of ASME for publication in the JOURNAL OF DYNAMIC SYSTEMS, MEASUREMENT, AND CONTROL. Manuscript received May 23, 2006; final manuscript received April 24, 2007; published online January 11, 2008. Review conducted by Rama K. Yedavalli.

3 Transcendental Transfer Function Approach

For many linear 1D diffusion systems, it is possible to analytically obtain a transcendental transfer function with an infinite number of poles,

$$\frac{Y(x,s)}{U(s)} = \frac{h(x,s)}{g(s)} \tag{2}$$

which we discretize to obtain a rational (polynomial) transfer function of order n.

3.1 Pole/Residue Series Truncation. We decompose Eq. (2) into a modal series by finding the poles p_k, with $g(p_k)=0$, unit step input steady state impedance

$$Z(x) = \lim_{s\to 0} \frac{h(x,s)}{g(s)} \tag{3}$$

and unit step residues

$$\mathrm{res}_k(x) = \lim_{s\to p_k} (s-p_k)Y(x,s) = \lim_{s\to p_k} (s-p_k)\frac{h(x,s)}{s\cdot g(s)} \tag{4}$$

Equation (4) is valid for nonrepeated p_k. The transcendental transfer function can be represented as the infinite series

$$\frac{Y(x,s)}{U(s)} = Z(x) + \sum_{k=1}^{\infty} \frac{\mathrm{res}_k(x)s}{s-p_k} \tag{5}$$

For step input $U(s)=u/s$, the time domain step response is

$$y(x,t) = u\left[Z(x) + \sum_{k=1}^{\infty} \mathrm{res}_k(x)e^{p_k t} \right] \tag{6}$$

An obvious method of representing a transcendental transfer function as a rational transfer function is to truncate Eq. (5) at n terms, yielding an nth order transfer function $Y^*(x,s)/U(s)$. Order n may be chosen using the following bandwidth or magnitude criteria:

(1) $p_n \approx -2\pi f_c$ $(p_1 > p_2 > \cdots > p_\infty)$ or
(2) $\|\mathrm{res}_n(x)\| < \alpha$ $(\|\mathrm{res}_1\| > \|\mathrm{res}_2\| > \cdots > \|\mathrm{res}_\infty\|)$.

3.2 Pole/Residue Truncation+Grouping. Transcendental transfer functions are commonly characterized by numerous closely spaced poles with similar residues. We partition the frequency range of interest into d "bins" and lump together modes within each bin. Grouping indices $k_f \subseteq \{0,1,2,\ldots,n\}$ are arranged such that $0=k_0<k_1<\cdots<k_d=n$. The grouped residue corresponding to bin $f\in\{1,2,\ldots,d\}$ is

$$\bar{\mathrm{res}}_f(x) = \sum_{k=k_{f-1}+1}^{k_f} \mathrm{res}_k(x) \tag{7}$$

with the corresponding residue-weighted pole

$$\bar{p}_f = \frac{\sum_{k=k_{f-1}+1}^{k_f} p_k \,\mathrm{res}_k(x_i)}{\bar{\mathrm{res}}_f(x_i)} \tag{8}$$

Residues in Eq. (8) are evaluated at a particular location x_i in the 1D domain. Equation (8) places the grouped pole near the mode with dominant response and allows closely spaced modes with opposite sign residues to cancel one another. The grouping procedure yields the dth order transfer function

$$\frac{Y^*(x,s)}{U(s)} = Z(x) + \sum_{f=1}^{d} \frac{\bar{\mathrm{res}}_f(x)s}{s-\bar{p}_f} \tag{9}$$

3.3 Pole/Residue Optimization. To assess the efficiency of the grouping method, we generate dth order ROMs in which optimal poles $\bar{\bar{p}}_f$ and residues $\bar{\bar{\mathrm{res}}}_{i,f}$ are found numerically to minimize the frequency response cost functional

$$J = \sum_{k=1}^{n_\omega}\sum_{i=1}^{n_x} |\mathrm{Re}(Y^*(x_i,j\omega_k) - Y(x_i,j\omega_k))|^2 + |\mathrm{Im}(Y^*(x_i,j\omega_k) - Y(x_i,j\omega_k))|^2 \tag{10}$$

Unlike Eq. (9), the numerical residues are found at discrete locations x_i and hold no connection to the analytical solution.

4 State Space Approach

When an analytical transfer function is inconvenient or unavailable, then a linear single-input multiple-output state space model with m states and m outputs,

$$\dot{\mathbf{x}} = \mathbf{A}\mathbf{x} + \mathbf{B}u$$

$$\mathbf{y} = \mathbf{C}\mathbf{x} + \mathbf{D}u \tag{11}$$

can be obtained using finite element or finite difference methods. We desire a ROM with n states $(n<m)$ and m outputs.

4.1 Eigenvalue/Residue Series Truncation. Similar to Sec. 3, the FOM transfer matrix can be represented in eigenvector/residue series form

$$\frac{\mathbf{Y}(s)}{U(s)} = \mathbf{Z} + \sum_{k=1}^{m} \frac{\mathbf{r}_k s}{s-\lambda_k} \tag{12}$$

The $m\times 1$ steady state vector is

$$\mathbf{Z} = -\mathbf{C}\mathbf{A}^{-1}\mathbf{B} + \mathbf{D} \tag{13}$$

We define the $m\times 1$ right eigenvector $\mathbf{q}_k$ with $\mathbf{A}\mathbf{q}_k=\lambda_k\mathbf{q}_k$ and the $1\times m$ left eigenvector $\mathbf{p}_k$ with $\mathbf{p}_k\mathbf{A}=\lambda_k\mathbf{p}_k$. Provided all eigenvalues of $\mathbf{A}$ are distinct and $\mathbf{p}_k\mathbf{q}_k=1$, the $m\times 1$ unit step input residue vector is

$$\mathbf{r}_k = \frac{\mathbf{C}\mathbf{q}_k\mathbf{p}_k\mathbf{B}}{\lambda_k} \tag{14}$$

The state space model [Eq. (11)] is transformed to modal form with

$$\hat{\mathbf{A}} = \mathrm{diag}[\lambda_1\ \lambda_2\ \cdots\ \lambda_m]$$

$$\hat{\mathbf{B}} = [1\ 1\ \cdots\ 1]^T$$

$$\hat{\mathbf{C}} = [\mathbf{r}_1\lambda_1\ \mathbf{r}_2\lambda_2\ \cdots\ \mathbf{r}_m\lambda_m]$$

$$\hat{\mathbf{D}} = \left[\mathbf{Z} + \sum_{k=1}^{m}\mathbf{r}_k\right] = \mathbf{D} \tag{15}$$

A detailed derivation of Eqs. (14) and (15) is given in a dissertation [18].

Again, we may reduce the mth order model by truncating Eq. (15) at n terms, yielding an nth order state space model defined with matrices $\mathbf{A}^*$, $\mathbf{B}^*$, $\mathbf{C}^*$, and $\mathbf{D}^*$ of dimensions $n\times n$, $n\times 1$, $m\times n$, and $m\times 1$, respectively.

4.2 Eigenvalue/Residue Truncation+Grouping. Similar to Sec. 3.2, We Define the $m\times 1$ grouped residue vector as

$$\bar{\mathbf{r}}_f = \sum_{k=k_{f-1}+1}^{k_f} \mathbf{r}_k \tag{16}$$

and the grouped eigenvalue as

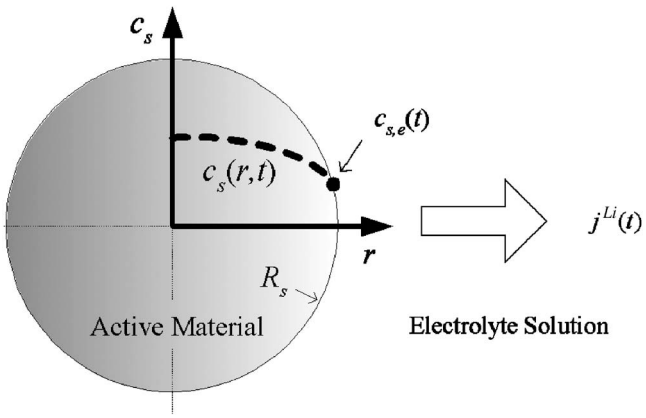

Fig. 1 Solid state diffusion problem for Li-ion cell

$$\bar{\lambda}_f = \frac{\sum_{k=k_{f-1}+1}^{k_f} \lambda_k r_{i,k}}{\bar{r}_{i,f}} \tag{17}$$

where $r_{i,k}$ corresponds to spatial location x_i. The grouping procedure yields a dth order state space model defined with matrices $\mathbf{A}^*$, $\mathbf{B}^*$, $\mathbf{C}^*$, and $\mathbf{D}^*$ of dimensions $d\times d$, $d\times 1$, $m\times d$, and $m\times 1$, respectively.

4.3 Eigenvalue/Residue Optimization. We numerically solve for optimal eigenvalues $\bar{\bar{\lambda}}_f$ and residue vectors $\bar{\bar{\mathbf{r}}}_f$ which minimize the error cost functional

$$J = \sum_{k=1}^{n_\omega} \sum_{i=1}^{n_x} |\mathrm{Re}(Y_i^*(j\omega_k) - Y_i(j\omega_k))|^2 + |\mathrm{Im}(Y_i^*(j\omega_k) - Y_i(j\omega_k))|^2 \tag{18}$$

where Y_i^* and Y_i are the ith outputs of the dth order ROM and the mth order FOM, respectively.

5 Examples

We illustrate the model order reduction technique using two examples arising from Li conservation within a 6 A h Li-ion hybrid electric vehicle (HEV) battery[19]. In the first example, solid state diffusion, we apply the model order reduction methods from Sec. 3 to an analytical solution. For the second example, electrolyte phase diffusion, composite geometry of the electrode/separator/electrode sandwich makes analytical treatment cumbersome. We use the finite element method to derive a state space model and reduce its order using the methods from Sec. 4.

5.1 Li-Ion Solid State Diffusion. A schematic of the solid state diffusion problem is shown in Fig. 1. The distribution of Li concentration $c_s(r,t)$ within a spherical electrode active material particle is described by

$$\frac{\partial c_s}{\partial t} = \frac{D_s}{r^2}\frac{\partial}{\partial r}\left(r^2\frac{\partial c_s}{\partial r}\right) \tag{19}$$

with symmetry at the particle center,

$$\left.\frac{\partial c_s}{\partial r}\right|_{r=0} = 0 \tag{20}$$

and a time-dependent boundary condition at the particle surface,

$$-D_s \left.\frac{\partial c_s}{\partial r}\right|_{r=R_s} = \frac{j^{\mathrm{Li}}(t)}{a_s F} \tag{21}$$

where D_s is the diffusion coefficient, $j^{\mathrm{Li}}(t)$ is the volumetric reaction current, a_s is the specific interfacial surface area, and F is Faraday's constant. We seek a ROM with input $j^{\mathrm{Li}}(t)$ and surface concentration output $c_{s,e}(t)=c_s(R_s,t)$.

Table 1 Solid state diffusion model parameters

Parameter	Value
Diffusion coefficient D_s (cm^2/s)	2.0×10^{-12}
Particle radius R_s (μm)	1.0
Specific interfacial area a_s (cm^2/cm^3)	17,400
Faraday's constant F (A s/mol)	96,487

From Eqs. (19)–(21), Jacobsen and West [20] found the transcendental transfer function

$$\frac{C_{s,e}(s)}{J^{\mathrm{Li}}(s)} = \frac{1}{a_s F}\left(\frac{R_s}{D_s}\right)\left[\frac{\tanh(\beta)}{\tanh(\beta)-\beta}\right] \tag{22}$$

with $\beta = R_s\sqrt{s/D_s}$. We remove the eigenvalue at the origin by subtracting off the bulk response $C_{s,\mathrm{av}}(s)/J^{\mathrm{Li}}(s) = -3/(R_s a_s F s)$. Defining $\Delta C_{s,e}(s) = C_{s,e}(s) - C_{s,\mathrm{av}}(s)$, the new transfer function

$$\frac{\Delta C_{s,e}(s)}{J^{\mathrm{Li}}(s)} = \frac{1}{a_s F}\left(\frac{R_s}{D_s}\right)\left[\frac{(\beta^2+3)\tanh(\beta)-3\beta}{\beta^2(\tanh(\beta)-\beta)}\right] \tag{23}$$

has finite steady state. Following model order reduction, the bulk response is reintroduced, giving a low order approximation to Eq. (23) that satisfies Li conservation.

Equation (23) is decomposed into a modal series following the procedure in Sec. 3.1. The poles of Eq. (23) are

$$p_k = -D_s\left(\frac{\xi_k}{R_s}\right)^2 \tag{24}$$

where ξ_k are roots of $\tan(\xi_k)=\xi_k$ not including $\xi_0=0$. The residues are

$$\mathrm{res}_k = \frac{-2}{a_s F R_s p_k} \tag{25}$$

and the steady state solution is

$$Z = \frac{-R_s}{5 a_s F D_s} \tag{26}$$

Substituting Eqs. (24)–(26) into Eq. (5) yields an infinite series transfer function algebraically equivalent to Eq. (23).

Property values used in the present model, defined in Table 1, are typical of solid state diffusion in electrochemical cells. The characteristic time $t \approx R_s^2/D_s = 5000$ s indicates that it can take over an hour for solid phase concentration gradients to relax. High power HEV batteries, however, may become solid state transport limited in as little as 5 s [19]. To capture these disparate time scales, we approximate dynamics from steady state to $f_c = 10$ Hz.

Figure 2 plots poles, Eq. (24), versus residues, Eq. (25), with the slowest pole (and largest residue) of the analytical solution located at -4.04×10^{-3} rad/s. Faster poles are spaced progressively closer together and, in the lower left corner of Fig. 2, discrete pole/residue pairs appear as almost a continuum of points. Retaining all poles $p_k > -20\pi$ yields a 178th order model, demonstrating that truncation (Sec. 3.1) can result in high model order.

The grouping approach (Sec. 3.2) is motivated by the observation that analytical poles in Fig. 2 are tightly spaced with similar residues. Brackets partition the real axis into d bins of equal logarithmic width, with the slowest bracket at $p_1/2$ and the fastest bracket at $-4\pi f_c$. Fifth order grouped pole/residue pairs, calculated with Eqs. (7) and (8), are plotted with circles in Fig. 2. Optimal pole/residue pairs, numerically identified by minimizing Eq. (10), share similar locations.

Figure 3 compares the frequency response of a truncated model and two grouped models with the exact frequency response, Eq. (23). The 180 term truncated series approximation matches the

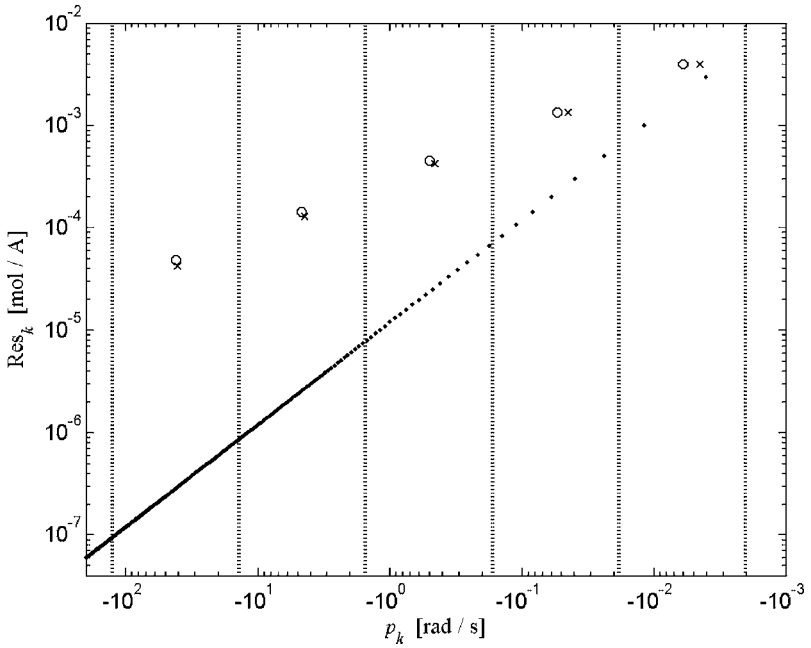

Fig. 2 Solid state diffusion poles and residues: Analytical (·), fifth order grouped (○), and fifth order optimal (×). Fifth order grouping brackets are shown with vertical dotted lines.

exact magnitude and phase until near 10 Hz where the phase angle diverges from the exact solution. Third and fifth order grouped models have similar characteristics, with the fifth order model producing a better match. The phase angle for the grouped models has the qualitative appearance of a curve fit.

Figure 4 compares the unit step response of a fifth order grouped model and a fifth order optimal model to a high order truncated "truth" model. Initially, the optimal model has a larger percentage error than the grouped model. The optimal error, however, more quickly decays to zero. The L^2 and L^∞ norms of surface concentration step response decrease with increasing model order for both types of ROMs [18]. Optimal models give slightly improved performance compared to grouped models but are more computationally expensive to identify.

5.2 Li-Ion Electrolyte Phase Diffusion. A schematic of the

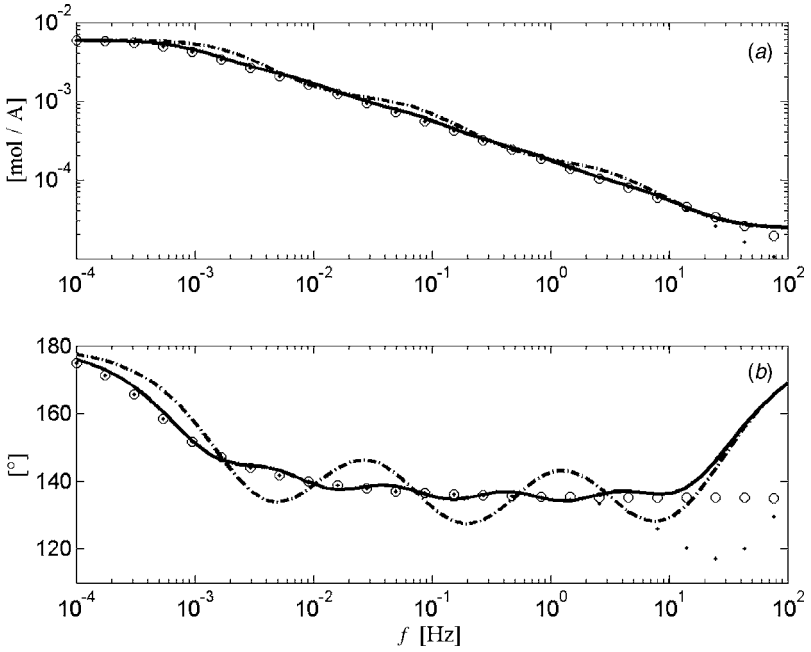

Fig. 3 Truncated and grouped solid state diffusion ROMs versus exact frequency response: Exact (○), 180th order truncated (·), 3rd order grouped (-·), and 5th order grouped (—). (*a*) Magnitude, $|\Delta C_{s,e}(s)/J^{\mathrm{Li}}(s)|$. (*b*) Phase angle, $\angle(\Delta C_{s,e}(s)/J^{\mathrm{Li}}(s))$.

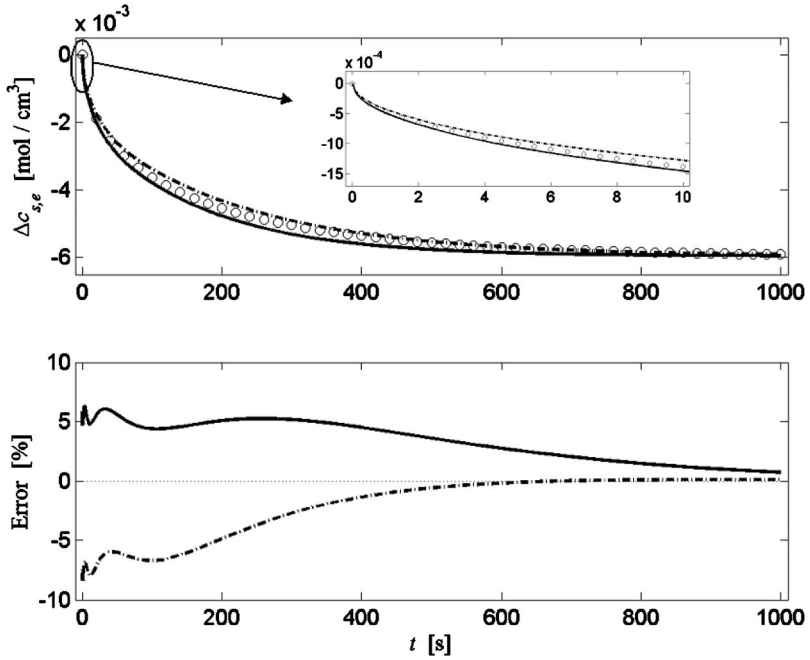

Fig. 4 Grouped and optimal solid state diffusion ROMs versus higher order model unit step response: 1000th order truncated (○), 5th order grouped (-), and 5th order optimal (--)

second example, electrolyte diffusion, is shown in Fig. 5. The distribution of electrolyte concentration $c_e(x,t)$ across the 1D Li-ion cell is described by

$$\frac{\partial(\varepsilon_e c_e)}{\partial t} = \frac{\partial}{\partial x}\left(D_e \frac{\partial}{\partial x} c_e\right) + \frac{1-t^o}{F} j^{\mathrm{Li}} \tag{27}$$

with zero flux conditions at the cell boundaries,

$$\left.\frac{\partial c_e}{\partial x}\right|_{x=0} = \left.\frac{\partial c_e}{\partial x}\right|_{x=L_{\mathrm{cell}}} = 0 \tag{28}$$

where ε_e is the electrolyte phase volume fraction, D_e is the diffusion coefficient, t^0 is the transference number, F is Faraday's constant, and j^{Li} is the current density of the electrochemical reaction at the solid/electrolyte interface. Model parameters are defined in Table 2. A Bruggeman relationship, $D_e = D_e^{\mathrm{ref}} \varepsilon_e^{1.5}$, corrects the reference diffusion coefficient for the tortuous path Li^+ ions follow through the porous media. We consider only the simple case of uniform current density across each electrode, allowing current density to equal total current I divided by electrode volume. Properties ε_e and D_e and source term j^{Li} have different values in the negative electrode, separator, and positive electrode regions, as follows:

$$D_{e-} = D_e^{\mathrm{ref}} \varepsilon_{e-}^{1.5} \quad j_-^{\mathrm{Li}} = \frac{I}{AL_-} \quad \text{(negative electrode)}$$

$$D_{e,\mathrm{sep}} = D_e^{\mathrm{ref}} \varepsilon_{e,\mathrm{sep}}^{1.5} \quad j_{\mathrm{sep}}^{\mathrm{Li}} = 0 \quad \text{(separator)}$$

$$D_{e+} = D_e^{\mathrm{ref}} \varepsilon_{e+}^{1.5} \quad j_+^{\mathrm{Li}} = \frac{-I}{AL_+} \quad \text{(positive electrode)}$$

Analytical treatment would require three individual solutions connected by concentration and flux matching conditions at the negative electrode/separator and separator/positive electrode interfaces. The finite element method is more convenient because the assembly process automatically satisfies internal matching conditions.

The $m \times 1$ vector $\mathbf{c}_e(t)$ approximates $c_e(x,t)$ at discrete node points, $x = x_i$, where $i \in \{1,2,\ldots,m\}$. The state space representation of Eq. (27) is

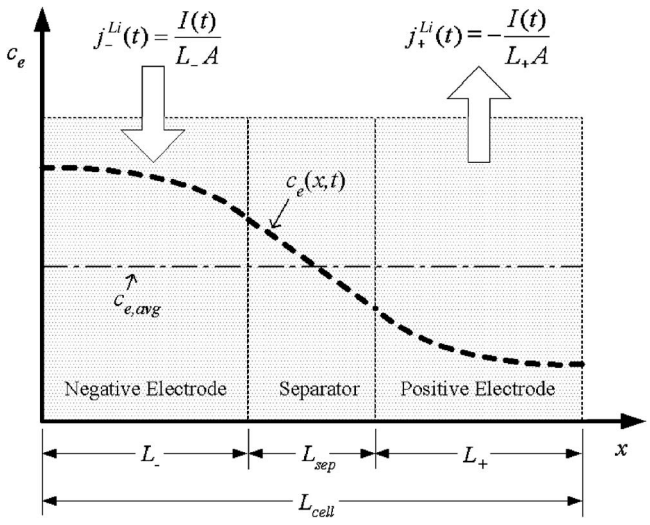

Fig. 5 Electrolyte phase diffusion problem for Li-ion cell with uniform reaction current distribution

Table 2 Electrolyte phase diffusion model parameters

Parameter	Value		
Diffusion coefficient D_e^{ref} (cm^2/s)		2.6×10^{-6}	
Transference number t^o		0.363	
Electrode plate area A (cm^2)		10,452	
	Negative electrode	Separator	Positive electrode
Porosity ε_e	0.332	0.5	0.330
Thickness L (μm)	50	25	43

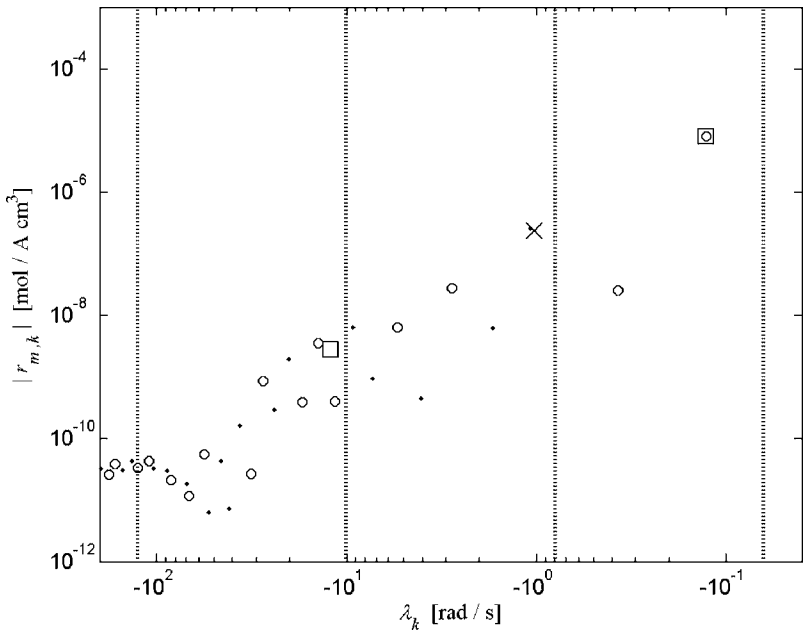

Fig. 6 Electrolyte phase diffusion eigenvalues and residues at $x=L_{cell}$: 45th order finite element $r_{m,k}>0$ (○) and $r_{m,k}<0$ (·) and 3rd order grouped $\bar{r}_{m,k}>0$ (□) and $\bar{r}_{m,k}<0$ (×). Third order grouping brackets are shown with vertical dotted lines.

$$\dot{\mathbf{c}}_e = -\mathbf{M}^{-1}\mathbf{K}\mathbf{c}_e + \mathbf{M}^{-1}\mathbf{F}I \tag{29}$$

where **M**, **K**, and **F** are the mass, stiffness, and forcing matrices, respectively [21]. To enforce species conservation and remove a pole/zero cancellation at the origin, we define a new field variable, $\Delta c_e(x,t)=c_e(x,t)-c_e(0,t)$, and Eq. (29) becomes

$$\Delta\dot{\mathbf{c}}_e = -(\mathbf{M}^{-1}\mathbf{K})_\Delta \Delta\mathbf{c}_e + (\mathbf{M}^{-1}\mathbf{F})_\Delta I \tag{30}$$

With states $\mathbf{x}=\Delta\mathbf{c}_e$, the $(m-1)$th order state variable model, Eq. (11), is defined by $\mathbf{A}=-(\mathbf{M}^{-1}\mathbf{K})_\Delta$, $\mathbf{B}=(\mathbf{M}^{-1}\mathbf{F})_\Delta$, $\mathbf{C}=\mathbf{I}$, and $\mathbf{D}=0$.

The present example spatially discretizes the 1D domain with 45 linear basis elements. It is common modeling practice to perform a grid independence test to check whether spatial discretization has been performed with a fine enough mesh. Results from a coarse mesh model are compared to those from a fine mesh model to validate the lower order model. Here, the grouping method efficiently produces low order models from the high order models

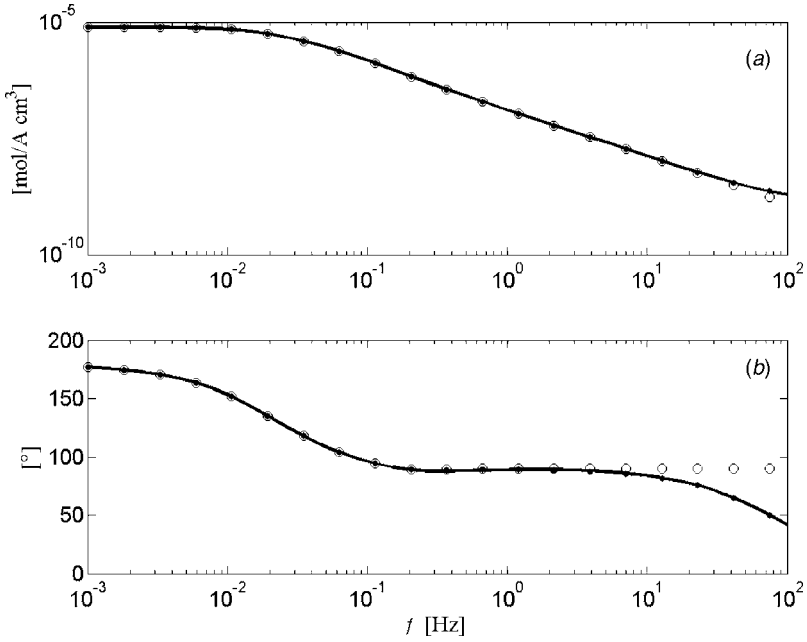

Fig. 7 Truncated and grouped electrolyte phase diffusion ROMs versus higher order model frequency response at $x=L_{cell}$: 45th order finite element (○), 28th order truncated (·), and 3rd order grouped (-). (*a*) Magnitude, $|\Delta C_e(L_{cell},s)/I(s)|$. (*b*) Phase angle, $\angle(\Delta C_e(L_{cell},s)/I(s))$.

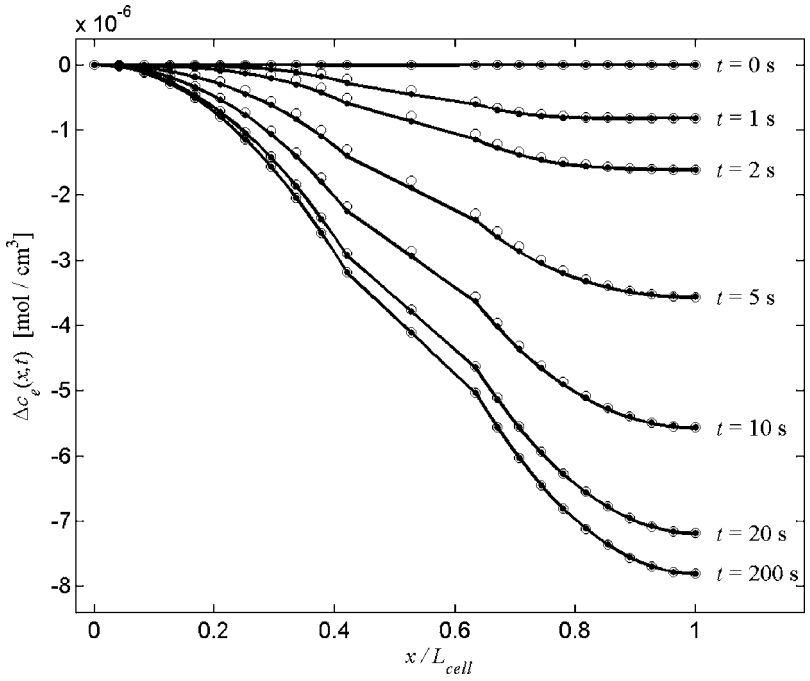

Fig. 8 Grouped and optimal electrolyte phase diffusion ROMs versus higher order model unit step response: 45th order finite element (○), 3rd order grouped (-), and 3rd order optimal (·)

associated with fine meshes.

Figure 6 plots eigenvalues of the **A** matrix versus residues, Eq. (14), at the location $x=L_{\text{cell}}$. To distinguish the sign of each residue on the log-log plot, Fig. 6 uses different symbols for residues with positive magnitude versus those with negative magnitude. In Eq. (27), the source term in the negative electrode is offset by a sink term in the positive electrode. Adjacent residues in Fig. 6 generally have alternating signs, causing near pole/zero cancellations and further motivating the grouping method. Figure 6 also shows eigenvalue/residue pairs corresponding to a third order grouped model.

Figure 7 compares the frequency response of a model truncated at 10 Hz and a third order grouped model with the FOM frequency response. Results shown are at $x=L_{\text{cell}}$, but the third order grouped model provides similar accuracy across the entire spatial domain. Figure 8 compares the unit step response of a third order grouped model and a third order optimal model with the full finite element model across the entire spatial domain. Small differences between the grouped and optimal models occur near the separator region.

The L_Ω^2 and L_Ω^∞ norms, evaluated from unit step response simulation results, are displayed in Table 3 and provide a quantitative metric of performance across the entire 1D domain. In general, the grouped residue models are near optimal and the grouped model performance improves as model order is increased. An exception is noted in Table 3, where the fourth order grouped model shows worse performance than the third order grouped model and is far from optimal. Here, our simple approach of partitioning the eigenspectrum with logarithmic evenly spaced brackets has not yielded the best possible fourth order grouped model. By manually adjusting the bracket placement, however, we are able to obtain other fourth order grouped models with near-optimal performance.

Table 3 Electrolyte phase diffusion ROM error norms

Model order	Reduction method	Electrolyte concentration (10^{-7} mol/cm^3)	
		L_Ω^∞	L_Ω^∞
2	Grouped	0.821	4.90
	Optimal	0.820	4.89
3	Grouped	0.1601	1.161
	Optimal	0.1435	1.098
4	Grouped	0.1618	1.167
	Optimal	0.0163	0.082

6 Conclusions

Residue grouping is a convenient method for combining closely spaced modes of a distributed parameter system with negative real eigenvalues. In traditional finite element or finite difference model grid generation, discretization presents a trade-off between model size and spatial resolution, with the former impacting execution speed and numerical stability. Using the approach in this paper to reduce the order of a model generated with very fine mesh grid, a low order model can be obtained with good spatial resolution.

Reduced order grouped models are shown to provide near-optimal performance, matching full order simulation results to within 6.3% for the fifth order solid state diffusion model and 1.2% for the third order electrolyte diffusion model. Compared to the 180th order truncated solid state diffusion model and the 45th order finite element electrolyte diffusion model, these grouped models execute 36 times and 15 times faster, respectively. The grouping procedure identifies these models using just 0.01 s and 0.07 s CPU times on a 1200 MHz Pentium III processor, compared to 8.1 s and 390 s, respectively, for the optimization procedure.

Model order reduction is performed in the frequency domain, and for control applications where only an approximate linear model is required [10], one may quickly obtain low order models with reasonable accuracy across a wide frequency range. Similar to the Karhunen–Loève Galerkin procedure [14], a high order analytical or numerical model is required; however, in the present

method, eigenvalue decomposition is performed directly on the model, rather than time simulation data, reducing computation and maintaining a tighter connection between the parameters of the full and reduced models.

Acknowledgment

This work was performed at the Pennsylvania State University Electrochemical Engine Center. The authors gratefully acknowledge funding provided by the U.S. Department of Energy Graduate Automotive Technology Education (G.A.T.E.) program through the Pennsylvania Transportation Institute.

References

[1] Chen, C. T., 1999, *Linear System Theory and Design*, Oxford University Press, New York.
[2] Jamshidi, M., 1983, *Large Scale Systems*, North-Holland, New York.
[3] Kokotovic, P. V., Khalil, H. K., and O'Reilly, J., 1986, *Singular Perturbations in Control: Analysis and Design*, Academic, London.
[4] Ray, W. H., 1981, *Advanced Process Control*, McGraw-Hill, New York.
[5] Theordoropoulou, A., Adomaitis, R. A., and Zafiriou, E., 1998, "Model Reduction for Optimization of Rapid Thermal Chemical Vapor Deposition Systems," IEEE Trans. Semicond. Manuf., **11**, pp. 85–98.
[6] Deng, H., Li, H. X., and Chen, G., 2005, "Spectral-Approximation-Based Intelligent Modeling for Distributed Thermal Processes," IEEE Trans. Control Syst. Technol., **13**, pp. 686–700.
[7] Doyle, M., Fuller, T., and Newman, J., 1993, "Modeling of Galvanostatic Charge and Discharge of the Lithium/Polymer/Insertion Cell," J. Electrochem. Soc., **140**, pp. 1526–1533.
[8] Um, S., Wang, C. Y., and Chen, K. S., 2000, "Computational Fluid Dynamics Modeling of Proton Exchange Membrane Fuel Cells," J. Electrochem. Soc., **147**, pp. 4485–4493.
[9] Christophides, P. D., and Daoutidis, P., 1997, "Finite Dimensional Control of Parabolic PDE Systems Using Approximate Inertial Manifolds," J. Math. Anal. Appl., **216**, pp. 398–420.
[10] Christophides, P. D., 2001, *Nonlinear and Robust Control of PDE Systems—Methods and Applications to Transport-Reaction Processes*, Birkhauser, Boston.
[11] Bhikkaji, B., and Söderström, T., 2001, "Reduced Order Models for Diffusion Systems Using Singular Perturbations," Energy Build., **33**, pp. 769–781.
[12] Bhikkaji, B., Mahata, K., and Söderström, T., 2004, "Reduced Order Models for a Two-Dimensional Heat Diffusion System," Int. J. Control, **77**, pp. 1532–1548.
[13] Bhikkaji, B., and Söderström, T., 2001, "Reduced Order Models for Diffusion Systems," Int. J. Control, **74**, pp. 1543–1557.
[14] Park, H. M., and Cho, D. H., 1996, "The Use of the Karhunen-Loève Decomposition for the Modeling of Distributed Parameter Systems," Chem. Eng. Sci., **51**, pp. 81–98.
[15] Loève, M., 1955, *Probability Theory*, Van Nostrand, Princeton, NJ.
[16] Sirovich, L., 1987, "Turbulence and the Dynamics of Coherent Structures, Parts I–III," Q. Appl. Math., **45**(3), pp. 561–590.
[17] Park, H. M., and Kim, O. Y., 2000, "A Reduction Method for the Boundary Control of the Heat Conduction Equation," ASME J. Dyn. Syst., Meas., Control, **122**, pp. 435–444.
[18] Smith, K. A., 2006, "Electrochemical Modeling, Estimation, and Control of Lithium Ion Batteries," Ph.D. thesis, The Pennsylvania State University, University Park.
[19] Smith, K., and Wang, C. Y., 2006, "Solid State Diffusion Effects on Pulse Operation of a Lithium Ion Cell for Hybrid Electric Vehicles," J. Power Sources, **161**, pp. 628–639.
[20] Jacobsen, T., and West, K., 1995, "Diffusion Impedance in Planar, Cylindrical and Spherical Geometry," Electrochim. Acta, **40**, pp. 255–262.
[21] Baker, A. J., and Pepper, D. W., 1991, *Finite Elements 123*, McGraw-Hill, New York.